

Journal Pre-proof

Optimizing graph neural network architectures for schizophrenia spectrum disorder prediction using evolutionary algorithms

Shurun Wang, Hao Tang, Ryutaro Himeno, Jordi Solé-Casals, Cesar F. Caiafa, Shuning Han, Shigeki Aoki, Zhe Sun



PII: S0169-2607(24)00412-7

DOI: <https://doi.org/10.1016/j.cmpb.2024.108419>

Reference: COMM 108419

To appear in: *Computer Methods and Programs in Biomedicine*

Received date: 26 November 2023

Revised date: 1 September 2024

Accepted date: 8 September 2024

Please cite this article as: S. Wang, H. Tang, R. Himeno et al., Optimizing graph neural network architectures for schizophrenia spectrum disorder prediction using evolutionary algorithms, *Computer Methods and Programs in Biomedicine* (2024), doi: <https://doi.org/10.1016/j.cmpb.2024.108419>.

This is a PDF file of an article that has undergone enhancements after acceptance, such as the addition of a cover page and metadata, and formatting for readability, but it is not yet the definitive version of record. This version will undergo additional copyediting, typesetting and review before it is published in its final form, but we are providing this version to give early visibility of the article. Please note that, during the production process, errors may be discovered which could affect the content, and all legal disclaimers that apply to the journal pertain.

© 2024 Published by Elsevier B.V.

Optimizing Graph Neural Network Architectures for Schizophrenia Spectrum Disorder Prediction Using Evolutionary Algorithms

Shurun Wang^{a,b}, Hao Tang^{a,g,*}, Ryutaro Himeno^b, Jordi Solé-Casals^{c,e}, Cesar F. Caiafa^d, Shuning Han^{c,f}, Shigeki Aoki^b, Zhe Sun^{b,*}

^a*School of Electrical Engineering and Automation, Hefei University of Technology, Hefei, 230009, China*

^b*Graduate School of Medicine, Juntendo University, Tokyo, 1138421, Japan*

^c*Data and Signal Processing Group, University of Vic—Central University of Catalonia, Vic, Catalonia, 08500, Spain*

^d*Instituto Argentino de Radioastronomía-CONICET CCT La Plata/CIC-PBA/UNLP, V. Elisa, 1894, Argentina*

^e*Department of Psychiatry, University of Cambridge, Cambridge, CB2 3EB, United Kingdom*

^f*Image Processing Research Group, RIKEN Center for Advanced Photonics, RIKEN, Wako-Shi, Saitama, Japan*

^g*Industrial Automation Engineering Technology Research Center of Anhui Province, Hefei, 230009, China*

Abstract

Background and Objective: The accurate diagnosis of schizophrenia spectrum disorder plays an important role in improving patient outcomes, enabling timely interventions, and optimizing treatment plans. Functional connectivity analysis, utilizing functional magnetic resonance imaging data, has been demonstrated to offer invaluable biomarkers conducive to clinical diagnosis. However, previous studies mainly focus on traditional machine learning methods or hand-crafted neural networks, which may not fully capture the spatial topological relationship between brain regions.

Methods: This paper propose an evolutionary algorithm (EA) based graph neural architecture search (GNAS) method. EA-GNAS has the ability to search for high-performance graph neural networks for schizophrenia spectrum disorder prediction. Moreover, we adopt GNNExplainer to investigate the explainability of the acquired architectures, ensuring that the model's predictions are both accurate and comprehensible.

Results: The results suggest that the graph neural network model, derived using genetic algorithm search, outperforms under five-fold cross-validation, achieving a fitness of 0.1850. Relative to conventional machine learning and other deep learning approaches, the proposed method yields superior accuracy, F1 score, and AUC values of 0.8246, 0.8438, and 0.8258, respectively.

Conclusion: Based on a multi-site dataset from schizophrenia spectrum disorder patients, the findings reveal an enhancement over prior methods, advancing our comprehension of brain function and potentially offering a biomarker for diagnosing schizophrenia spectrum disorder.

Keywords: Graph neural network, graph neural architecture search, evolutionary algorithm, schizophrenia spectrum disorder, brain functional connectivity.

1. Introduction

Schizophrenia spectrum disorder (SSD) is a serious mental illness that ranks among the leading causes of disability and affects more than twenty million individuals globally [1]. Individuals diagnosed with SSD often face challenges in integrating with their communities. They have a low quality of life due to the severe impairment in social and occupational functioning, often exacerbated by persistent delusions, hallucinations, and cognitive deficits [2]. An accurate diagnosis of SSD allows patients to receive timely and appropriate treatment and support, improving their quality of life, alleviating social functional barriers, and reducing the psychological and economic burdens on families. Therefore, developing an accurate SSD diagnostic method has significant clinical importance and also brings positive benefits to societal health and well-being.

In recent years, research on SSD has concentrated on understanding the underlying brain abnormalities and mechanisms through morphological and neurobiological characteristics. Several prevalent neuroimaging techniques, including functional magnetic resonance imaging (fMRI), magnetoencephalography (MEG), positron emission tomography (PET), and magnetic resonance spectroscopy (MRS), are utilized for brain structure and function analysis in individuals with SSD [3, 4, 5]. Among them, resting-state fMRI (rs-fMRI) is primarily used to measure blood oxygen level-dependent signals in the brain at rest. This technique does not require any specific task stimulation but records brain activity in its resting state. Researchers have found that brain functional connectivity (FC) constructed using rs-fMRI can distinguish between the SSD group and the healthy group [6, 7, 8]. Hence, how to design robust classification methods based on brain FC is a topic of interest for many researchers currently.

For over a decade, traditional machine learning (ML) techniques have played a pivotal role in brain network classification. The support vector machine (SVM), a supervised technique, is the most prevalently used ML method in this field. Ma *et al.* employed SVM to classify 44 schizophrenia patients and 40 healthy controls, achieving an accuracy of 0.8137 [6]. Ramkiran *et al.* employed the anticorrelation after mean of Antilog (AMA) method to simplify the fully connected FC matrices. Subsequently, they utilized SVM for classifying 112 subjects, achieving an average accuracy of 0.74 [9]. Gao *et al.* assessed the utility of the amplitude of low-frequency fluctuation (ALFF) via SVM as a means of diagnosing SSD [10]. Besides SVM, other ML methods, such as logistic regression (LR) and random forests (RF), are also mentioned in some SSD prediction approaches. Srinivasagopalan *et al.* utilized independent component analysis for feature selection and subsequently integrated it with the LR and RF techniques. In the classification of 75 controls

*Corresponding author

Email addresses: htang@hfut.edu.cn (Hao Tang), z.sun.kc@juntendo.ac.jp (Zhe Sun)

30 and 69 patients, they achieved accuracies of 0.8277 and 0.8333, respectively [11]. In [12], features were
31 extracted from the gray matter volume (GMV) and ALFF. Then, the Xgboost classifier, combined with the
32 information fusion method, was employed to identify 38 healthy controls, 16 deficit schizophrenic patients,
33 and 31 non-deficit schizophrenic patients. These examples exhibit the practical applications of various ML
34 methods. However, the quality and relevance of feature selection profoundly impact the performance of ML,
35 and biased feature extraction can lead to imprecise class discrimination [13, 14].

36 Unlike traditional ML techniques, deep learning (DL) obviates the need for complex feature engineering
37 and strives to establish an end-to-end model for data processing and prediction. It has garnered increasing
38 popularity for diverse biomedical applications, including medical image analysis and disease prediction [15,
39 16]. The BrainNetCNN, proposed in [17], is a convolutional neural network (CNN) framework designed
40 for predicting clinical neurodevelopmental outcomes based on brain networks. This framework leverages
41 the topological locality inherent in structural brain networks and has demonstrated effectiveness in recent
42 biomedical engineering approaches [18, 19, 20]. Moreover, brain FC is essentially the graph-structured data,
43 where nodes signify brain regions and edges denote either the structural or functional link between these
44 regions. Therefore, several studies have employed the graph neural network (GNN), a powerful DL model
45 capable of generating embeddings for a node by aggregating features from its neighboring nodes, for tasks
46 such as node classification, graph classification, or link prediction. Chen *et al.* utilized a graph convolutional
47 network (GCN) to classify schizophrenia patients based on brain region and connectivity features extracted
48 from a combined functional MRI and connectomics analysis [21]. Yu *et al.* proposed an improved graph
49 attention network (GAT) with the bilinear convolution for diagnosis of schizophrenia [22]. GNN-based
50 methods are also been employed in the diagnosis of other diseases, including autism spectrum disorder
51 (ASD) and major depressive disorder (MDD) [23, 24]. Han *et al.* proposed the FCbasedGCN model for the
52 early prediction of dementia using fMRI data [25]. Zhang *et al.* proposed the LGGNN model to achieve the
53 precise classification of ASD [26]. Although researchers can optimize the network to enhance recognition
54 accuracy, it is necessary to test the effects of a large number of GNN components (such as convolutional
55 layers, aggregators, and activation functions). This requires researchers to have a deep understanding of
56 network architecture design and a substantial time investment. Thus, how to effectively determine the
57 proper GNN architecture from numerous design choices presents a significant challenge.

58 Neural architecture search (NAS) can automatically seek high-performance deep neural networks (DNN),
59 and it has achieved remarkable advancements in many fields such as computer vision [27] and natural
60 language processing [28] in recent years. Unlike NAS, GNAS is designed to generate the optimal GNN

61 model for extracting features from graph-structured data. Through the establishment of a predefined search
62 space, GNAS enables the efficient exploration of possible architectures, the assessment of their performance,
63 and the systematic refinement of the search process grounded in acquired knowledge, ultimately yielding
64 the ideal model. To date, most of the GNAS methods are based on reinforcement learning (RL) and EA.
65 RL-based GNAS methods (e.g., GraphNAS [29], Auto-GNN [30]) generally require training a controller to
66 generate component strings describing the structure of GNN. However, training both the controller and
67 the GNN model simultaneously requires more computational time. Additionally, the controller typically
68 generates candidate GNN models in a sequential manner, making it difficult to scale to a large search space
69 and perform parallel model evaluations. EA-based GNAS methods employ an iterative process whereby
70 individuals (i.e., GNN models) are selected from an initialized population and evaluated according to a
71 fitness function. Subsequently, a new population is generated using the best-performing individual from
72 the preceding generation. Since all individual models in the population are independent, EA-based GNAS
73 methods can be easily scaled to a large search space and models can be evaluated simultaneously. AGNAS
74 [31] employs a genetic algorithm for the GNAS process and evaluates individuals in parallel, yet it does not
75 treat the optimizer as a hyper-parameter in the search space. Genetic-GNN [32] includes the optimizer in
76 the search space, but the GNN search process remains limited by the genetic algorithm framework. There
77 are certain obstacles when attempting to extend to other advanced evolutionary algorithms.

78 To address the aforementioned problems, this paper proposes a novel GNAS framework, named EA-
79 GNAS. It identifies the optimal model through a search within a vast GNN architecture space, and the model
80 is applied for SSD prediction. Different from the exiting GNAS methods that utilize the specific evolutionary
81 algorithm, EA-GNAS is designed to be generic and adaptable to various evolutionary algorithms, enabling a
82 more flexible and comprehensive exploration of the GNN architecture space. Unlike existing SSD prediction
83 methods, the SSD prediction model proposed in this paper is obtained through an automated search process,
84 rather than traditional manual design. The advanced GNAS technology allows for the automatic exploration
85 of the model structure most suitable for specific tasks, which not only reduces the professional knowledge and
86 time cost required to design effective models but also discovers innovative solutions that might be overlooked
87 by manual design methods in a broad architectural space. Moreover, although many studies use DL models
88 to predict SSD, they usually only report the performance of the model without detailing which features
89 within brain FC significantly influence the prediction outcomes. Therefore, to achieve more accurate SSD
90 predictions and a clearer understanding of the underlying factors, it is necessary to develop a robust GNN
91 model and undertake explainability analysis for the model. The principle contributions of this paper are

92 listed as follows:

93 (1) We propose a novel generic evolutionary GNAS framework named EA-GNAS, designed to automati-
94 cally identify high-performance GNN architectures from a well-defined search space. Within this framework,
95 six popular evolutionary algorithms are compared to evaluate their search performance in the task of SSD
96 prediction.

97 (2) We utilize a GNN explainability analysis method, GNNExplainer, to conduct in-depth exploration
98 and explanation of the searched GNN model. Through this approach, the most critical brain region features
99 can be identified, allowing for a detailed understanding of the neural mechanisms that significantly contribute
100 to SSD prediction.

101 (3) In comparison with four ML-based and six DL-based methods tested on multi-site SSD datasets, our
102 proposed method demonstrates superior performance across several metrics. The source code is publicly
103 available on GitHub at <https://github.com/Shurun-Wang/EA-GNAS>.

104 2. Problem definition

105 The purpose of this paper is to propose a framework for searching graph neural network architectures
106 based on evolutionary algorithms, and to apply the discovered optimal network to predict SSD. Additionally,
107 we employ a graph-based explainability method to explain the prediction results. Therefore, the problem
108 definition can be categorized into three aspects: GNN-based disease prediction, GNAS, and graph explain-
109 ability.

110 **Definition 1** (*GNN-based disease prediction*): The objective of GNN-based disease prediction is to
111 classify the specific property of interest for an entire graph $\mathcal{G} = (\mathcal{V}, \mathcal{E})$, where $\mathcal{V} = \{v_i\}_{i=1,2,\dots,V}$ is a set
112 of V unique nodes and $\mathcal{E} = \{e_{i,j}\}_{i,j=1,2,\dots,V;i \neq j}$ is a set of edges. Specifically, edges can be represented by
113 a binary adjacency matrix of size $V \times V$, where $A_{i,j} = 1$ when $e_{i,j} \in \mathcal{E}$, otherwise $A_{i,j} = 0$. In addition,
114 $\mathcal{F} \in \mathbb{R}^{V \times F}$ is a feature matrix containing all V nodes with their associate F features. In this work, the
115 brain function connectivity of each subject forms a graph, with each brain region represented as a node, the
116 connection between two brain regions represented as an edge, and the correlations between a brain region
117 and other brain regions serving as node features. Therefore, for M subjects, we obtain the input space of
118 graphs $\{\mathcal{G}_m\}_{m=1,2,\dots,M}$ and a set of class labels \mathcal{Y} (i.e., disease types). The objective of the classification
119 task is to learn a mapping function $\mathbf{p} : \{\mathcal{G}_m\}_{m=1,2,\dots,M} \rightarrow \mathcal{Y}$, and \mathbf{p} is the GNN model derived by GNAS.

120 **Definition 2** (*GNAS*): The graph set $\{\mathcal{G}_m\}_{m=1,2,\dots,M}$ can be partitioned into training set \mathcal{D}_{train} , vali-
121 dation set \mathcal{D}_{val} , and test set \mathcal{D}_{test} . Given a predefined collection containing all graph neural architectures

122 \mathcal{P} , GNAS aims to find an optimal neural architecture $\mathbf{p}^* \in \mathcal{P}$, so that the model can be trained on \mathcal{D}_{train}
 123 to achieve the best performance, thereby minimizing the fitness on \mathcal{D}_{val} . Formally, it can be represented as
 124 a following bi-level optimization problem:

$$\begin{cases} \mathbf{p}^* = \arg \min_{\mathbf{p} \in \mathcal{P}} \mathcal{L}_1(\mathbf{p}(\omega^*), \mathcal{D}_{val}) \\ \text{s.t.} : \omega^* = \arg \min_{\omega} \mathcal{L}_2(\mathbf{p}(\omega), \mathcal{D}_{train}) \end{cases} \quad (1)$$

125 Here, \mathbf{p} denotes a graph architecture generated by a search method, ω is the weights of the model \mathbf{p} , $\mathcal{L}_2(\cdot)$
 126 is the training loss, and $\mathcal{L}_1(\cdot)$ (i.e., the fitness of the search method) measures the performance of \mathbf{p} on \mathcal{D}_{val} .
 127 Finally, the generalization performance of the optimal model \mathbf{p}^* is evaluated on \mathcal{D}_{test} .

128 **Definition 3** (*Graph explainability*): For a specific graph $\mathcal{G} = (\mathcal{V}, \mathcal{E})$ and feature matrix \mathcal{F} , the goal of
 129 the graph explainability is to identify and score the parts of \mathcal{G} and \mathcal{F} that are most influential in the model's
 130 prediction for graph-level classification. In this study, the important brain regions and the connectivity
 131 relationships are defined as \mathcal{G}_s , and the crucially features are given as \mathcal{F}_s .

132 3. Preliminaries

133 In this section, we separately introduce the preliminary knowledge about graph neural networks, evolu-
 134 tionary algorithms, and the GNNExplainer method.

135 3.1. Graph neural networks

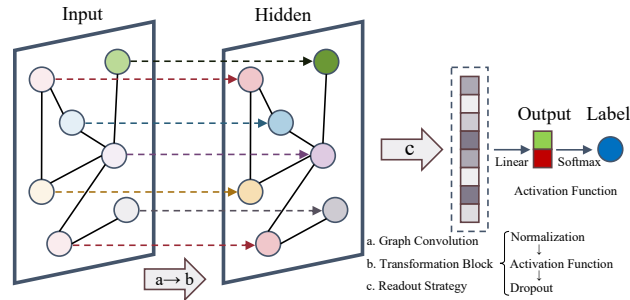


Figure 1: The illustration of the general GNN framework for graph classification.

136 GNN is a category of neural network models capable of directly integrating graph topology and node
 137 attributes to facilitate efficient learning of graph representation. Fig. 1 illustrates a typical schematic of

138 using GNN for graph-level binary classification on a graph, and the model contains the following three basic
 139 GNN structure components:

140 a. **Graph Convolution.** Most popular graph convolution operations employ a neighbor aggregation (or
 141 message-passing) mechanism, where the updating of node features initially involves aggregating messages
 142 from neighboring nodes of the current node, followed by combining the aggregated messages with the node’s
 143 own features. The updating process of the l -th graph convolution layer for each node $v \in \mathcal{V}$ is formulated
 144 as:

$$\begin{cases} \mathbf{a}_v^{(l)} = \text{AGGREGATE}^{(l)} \left(\left\{ \mathbf{f}_u^{(l-1)} : u \in \mathcal{N}(v) \right\} \right) \\ \mathbf{f}_v^{(l)} = \text{COMBINE}^{(l)} \left(\mathbf{f}_v^{(l-1)}, \mathbf{a}_v^{(l)} \right) \end{cases}, \quad (2)$$

145 where $\mathcal{N}(v)$ represents the set of all neighboring nodes of node v . $\mathbf{a}_v^{(l)}$ and $\mathbf{f}_v^{(l)}$ are the message vector and
 146 feature vector of node v at the l -th layer, respectively. Most graph convolutions such as GCN [33], Graph-
 147 SAGE [34], GAT [35], and others can be implemented within this framework through various aggregation
 148 and combination mechanisms.

149 b. **Transformation Block.** This block is comprised of normalization, activation function, and dropout,
 150 designed in sequence to enhance the model’s performance. Normalization involves scaling node features,
 151 which improves the training stability and convergence. Typical normalization methods include batch nor-
 152 malization, layer normalization, among others. Activation functions like ReLU and Sigmoid introduce
 153 non-linearity into the model, aiding in capturing intricate patterns and relationships in graph-structured
 154 data. Dropout is a regularization technique that, during network training, randomly sets a node’s hid-
 155 den representation to zero with a probability p , aimed at preventing overfitting and improving the model’s
 156 generalization capacity.

157 c. **Readout Strategy.** In graph-level tasks, after updating the node features \mathbf{f}_v within the graph, it is
 158 typically necessary to employ a readout strategy to aggregate the information of the entire graph structure
 159 into a single feature vector \mathbf{h} . This process can be described as follows:

$$\mathbf{h} = \text{READOUT}(\{\mathbf{f}_v, v \in \mathcal{V}\}). \quad (3)$$

160 Commonly used readout strategies include mean, sum, max, and others [36]. Different readout strategies
 161 have varying effects on the fusion of node features within the entire graph.

162 3.2. Evolutionary algorithms

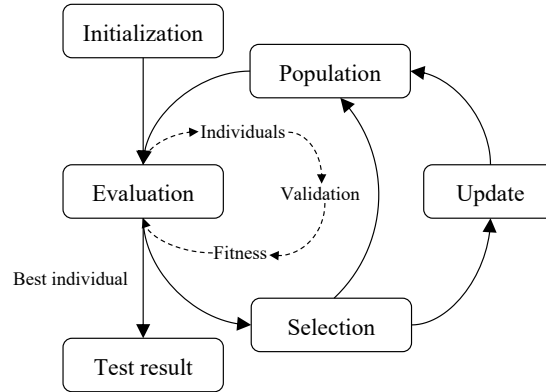


Figure 2: The typical optimization cycle of evolutionary algorithm.

163 Evolutionary algorithms are a family of population-based meta-heuristic optimization method, which is
 164 originally inspired by the process of evolution in nature. In general, most existing evolutionary algorithms
 165 (e.g., genetic algorithms [37], particle swarm optimization [38], etc.) share a common framework, as illus-
 166 trated in Fig. 2, primarily consisting of five components: initialization, evaluation, selection, update, and
 167 testing. Specifically, the population represents a collection of candidate individuals, and the selection and
 168 update operations continuously iterate the population, selecting the best individual based on evaluation
 169 criteria for testing. In the context of evolutionary neural architecture search, each individual represents a
 170 specific neural network model, typically measured by its accuracy on a validation dataset, referred to as the
 171 fitness value. Throughout the evolution process, environmental selection incorporates evaluated individuals
 172 into the population, while underperforming models are eliminated. Furthermore, updating the evaluated
 173 individuals ensures the diversity of the population. Through the continuous iteration of the evolutionary
 174 population, the model with the best performance in the final population will be used for practical testing
 175 tasks.

176 3.3. GNNExplainer method

177 After training the model obtained through the GNAS process, it is insightful to identify the brain
 178 regions that are critical for the final prediction. GNNExplainer, proposed by Ying et al. [39], is employed
 179 to obtain the significant subgraph through graph masking. The main idea is to obtain the subgraph \mathcal{G}_s and
 180 its associated features \mathcal{F}_s by masking the relevant part of the input entire graph. The mask is determined
 181 through an optimization algorithm that iteratively seeks to identify the subgraph that maximizes the mutual

182 information objective:

$$\max_{\mathcal{G}_s} MI(\mathbf{Y}, (\mathcal{G}_s, \mathcal{F}_s)) = H(\mathbf{Y}) - H(\mathbf{Y}|\mathbf{G} = \mathcal{G}_s, \mathbf{F} = \mathcal{F}_s), \quad (4)$$

183 where \mathbf{Y} represents the predicted label distribution. Random variables are represented by bold letters, while
 184 their instantiations are indicated by non-bold letters.

185 4. The proposed method

186 This section presents EA-GNAS framework to evolve the GNN model. We first define the search space
 187 for GNN, then outline the working principle of EA-GNAS. Subsequently, we provide a detailed description
 188 of the implementation process, and finally introduce performance evaluation metrics and some comparison
 189 methods.

190 4.1. Search space

191 In general, a complete GNN model is composed of multiple components, and the combination of different
 192 components can affect the model’s performance. Additionally, different optimizers can also lead to variations
 193 in the training results of the model. To ensure that the evolutionary algorithm can search for suitable GNN
 194 models, we need to define the search space (Ω) for network components and optimizers, as described in
 195 Table 1. In the search space, there are nine components: c_1 to c_6 represent convolution type, channel,
 196 normalization, activation function, dropout, and readout, respectively. These components are essential for
 197 constructing a GNN. Different combinations of these components within the search space can generate
 198 various GNN models. o_1 , o_2 , and o_3 represent the optimizer, learning rate, and weight decay, respectively,
 199 used for training the GNN model. Specifically, a total of six different graph convolutional types (c_1) are
 200 selected to learn node features. Among them, GraphConv [33] employs spectral-based convolutional filters
 201 to recursively aggregate information from all the direct neighbors of each node and utilizes this information
 202 to update the features of each node. ChebConv [40] utilizes the Chebyshev polynomial basis to represent the
 203 spectral-based convolutional filters. SAGEConv [34] is a general inductive framework that uses node features
 204 to efficiently generate node embeddings for previously unseen data. GATConv [35] incorporates a masked
 205 self-attention mechanism, which assigns appropriate weights to various neighboring nodes, thereby directing
 206 attention towards nodes of greater significance while attenuating the influence of nodes with comparatively
 207 lesser relevance. ResGatedGraphConv [41] introduces residual connections and recurrent neural networks
 208 into graph convolution, enabling it to handle variable-length graph tasks. Meanwhile, the number of output

209 channels (c_2) in graph convolution determines the output dimensionality of node features, and we offer a
 210 total of seven selectable options. Furthermore, the search space encompasses three common normalization
 211 methods (c_3), five activation functions (c_4), and five different dropout rates (c_5), where 'None' indicates
 212 that the component is not selected. In the readout strategy (c_6), five statistical methods are employed to
 213 aggregate node features into graph features. Finally, three commonly used optimizers (i.e., Adam, SGD,
 214 and RMSprop) (o_1), along with different learning rates (o_2) and weight decay rates (o_3), are provided as
 215 candidate components for training the GNN model.

Table 1: The search space for GNN components and optimizer.

Components	Search space (Ω)
Convolution type (c_1)	GraphConv, ChebConv, SAGEConv, GATConv, ResGatedGraphConv
Channel (c_2)	4, 8, 16, 32, 64, 128, 256
Normalization (c_3)	None, Batch Normalization, Layer Normalization, Instance Normalization
Activation (c_4)	None, Sigmoid, Tanh, ReLU, ELU, Leaky ReLU
Dropout (c_5)	None, 0.1, 0.2, 0.3, 0.4, 0.5
Readout (c_6)	Sum, Mean, Max, Var, Std
Optimizer (o_1)	Adam, SGD, RMSprop
Learning rate (o_2)	1e-2, 1e-3, 1e-4
Weight decay (o_3)	1e-3, 1e-4, 1e-5

216 4.2. EA-GNAS

217 To describe the architecture of GNN clearly, we treat the components c_1 to c_5 within the GNN as a single
 218 graph convolution block and represent all the components to be searched as a tuple. Assuming we search
 219 for the optimal model with L graph convolution blocks, the architecture \mathbf{p} can be represented as follows:

$$\mathbf{p} = (c_1^{(1)}, c_2^{(1)}, c_3^{(1)}, c_4^{(1)}, c_5^{(1)}, \dots, c_1^{(L)}, c_2^{(L)}, c_3^{(L)}, c_4^{(L)}, c_5^{(L)}, c_6, o_1, o_2, o_3), \quad (5)$$

220 where the first block and last blocks are indexed by (1) and (L), respectively. It is worth noting that the
 221 variables in \mathbf{p} are discrete, so some evolution algorithms based on continuous space position updates, such
 222 as PSO and snake optimization (SO) [42], cannot be directly applied to GNAS. To address this issue, we
 223 implement a floor operation following the position updates in the evolutionary algorithm, resulting in an
 224 integer value that uniquely corresponds to the candidate positions of the components within the search
 225 space. The proposed generic GNAS framework based on EA is shown in Algorithm 1.

Algorithm 1 A generic graph neural architecture search algorithm based on evolutionary algorithm.

Input: The hyper-parameter set Φ of EA, graph block number L , learning iteration N , individual number I , search space Ω , training set \mathcal{D}_{train} , validation set \mathcal{D}_{val} , architecture memory $\mathcal{P} \leftarrow \emptyset$.

Output: The best architecture \mathbf{p}^* in \mathcal{P}

- 1: Obtain the lower bound \mathbf{lb} and upper bound \mathbf{ub} through L and Ω
 - 2: Initialize the individuals $\mathbf{S} \leftarrow \text{Uniform}(\mathbf{lb}, \mathbf{ub})$
 - 3: **for** iteration = 1 to N **do**
 - 4: Obtain all architectures \mathbf{P} through decoding \mathbf{S}
 - 5: **for** $i = 1$ to I **do**
 - 6: Construct the GNN models according to $\mathbf{p}_i \in \mathbf{P}$
 - 7: $\mathcal{P} \leftarrow \mathcal{P} \cup \mathbf{p}_i$
 - 8: Compute the fitness $\phi_i \leftarrow 1 - \text{CrossValidation}(\mathbf{p}_i, \mathcal{D}_{train}, \mathcal{D}_{val})$
 - 9: **end for**
 - 10: Update $\mathbf{S} \leftarrow \text{EA}(\Phi, \mathbf{S}, \phi)$
 - 11: Limit boundary $\mathbf{S} \leftarrow \text{Limit}(\mathbf{S}, \mathbf{lb}, \mathbf{ub})$
 - 12: **end for**
-

226 The algorithm’s inputs include the hyper-parameter set Φ of the evolutionary algorithm, the hyper-
 227 parameters (L, N, I) for training the GNN model, and the training and validation sets. Among them, Φ
 228 represents the specific hyper-parameters of different evolutionary algorithms, such as the crossover rate and
 229 mutation rate for GA, and the cognitive factor, social factor, and inertia weight for PSO. The algorithm’s
 230 output is the optimal architecture \mathbf{p}^* with the best performance in the architecture memory \mathcal{P} . The
 231 algorithm initializes a population of individuals using a uniform distribution within the search space, and
 232 then iteratively updates the population using the evolutionary algorithm. In each iteration, the algorithm
 233 decodes the individuals to obtain a set of GNN architectures, constructs the corresponding models, and
 234 evaluates their fitness using cross-validation on the training and validation sets. The fitness values are then
 235 used to update the population using the EA algorithm, which searches for the optimal architecture. The
 236 algorithm terminates after N iterations, and the best architecture is selected from the final population.

237 Moreover, several important considerations are worth mentioning. First, when we have a graph block
 238 number denoted as L , it’s essential to note that the dimensions of the lower and upper bounds for optimiza-
 239 tion variables are identical, each being $5L+4$. Specifically, $\mathbf{lb} = (0, 0, \dots, 0)$, and $\mathbf{ub} = (ub_1, ub_2, \dots, ub_{5L+4})$.
 240 Here, the i -th upper bound element in \mathbf{ub} is represented as ub_i , which is equal to the candidate number of
 241 the i -th component in (5). Secondly, we randomly select a set of I individuals from the interval between
 242 \mathbf{lb} and \mathbf{ub} , and we represent this population as $\mathbf{S} = \{\mathbf{s}_i | i \in [1, I], i \in \mathbb{N}^+\}$. During the construction of the
 243 GNN model, the decoding process includes rounding down each individual $\mathbf{s}_i \in \mathbb{R}^{5*L+4}$, and this resulting
 244 integer value serves as an index for the search space Ω . Finally, the evolutionary algorithm will iteratively

245 update the population \mathbf{S} while limiting upper and lower bounds throughout N iterations.

246 *4.3. Dataset construction*

Table 2: Demographic characteristics of subjects included in the SRPBS Dataset.

	Site	Healthy group	SSD group
KTT	No., M:W	75, 48:27	44, 25:19
	Age	28.9 (9.1)	37.3 (9.7)
KUT	No., M:W	159, 93:66	44, 20:24
	Age	36.5 (13.6)	41.3 (10.9)
SWA	No., M:W	101, 86:15	19, 15:4
	Age	28.4 (7.9)	42.9 (8.4)
UTO	No., M:W	170, 78:92	35, 23:12
	Age	35.6 (17.5)	31.7 (10.4)

M, men; W, women

247 The rs-fMRI datasets in this study were obtained from the Japanese Strategic Research Program for the
 248 Promotion of Brain Science (SRPBS) dataset 1 [43]. This dataset consists of 142 SSD patients (83 men versus
 249 59 women) and 505 health subjects (305 men versus 200 women) from 4 sites (KTT, KUT, SWA, and UTO).
 250 Subject demographics information are listed in Table 2, and data are shown as means (standard deviation).
 251 The brain features pertaining to individual subjects, specifically functional connectivities (FC), were derived
 252 from 10-minute rs-fMRI BOLD signals that had undergone identical transformation procedures. The pro-
 253 cedures include slice-time correction, realignment, co-registration, segmentation of T1-weighted structural
 254 images, normalization to the Montreal Neurological Institute space, and spatial smoothing using an isotropic
 255 Gaussian kernel with a 6 mm full-width at half-maximum. In order to calculate these subject-specific func-
 256 tional connectivities, the BrainVISA Sulci Atlas parcellation scheme was utilized, which subdivided each
 257 individual image into 140 regions as detailed by Perrot *et al.* [44]. For the extraction of time series data and
 258 the computation of the connectivity matrix, the standard Pearson correlation coefficient (PCC) method was
 259 employed. As a result, 9,730 connectivity features were computed for each subject, thereby constituting a
 260 weighted brain feature matrix with dimensions [647, 140, 140].

261 FC data contains a large amount of feature information, but too much information can cause feature
 262 redundancy and prolong training time. Therefore, effective preprocessing of FC data is crucial for the GNAS
 263 process. After data collection, we performed a series of data preprocessing steps to construct a graph dataset
 264 suitable for training GNN models. First, we randomly partitioned all subjects into training and test sets in
 265 a 4:1 ratio. Then, we averaged the FC matrices of all training set and used minimum spanning trees (MST)

266 [45] to search for nodes in the averaged graph. The threshold of MST is used to control the scale of the
 267 generated minimum spanning tree to filter out important connection relationships. Next, we transformed the
 268 results of MST into binary form, creating a binary adjacency matrix, which serves as the node connectivity
 269 for the graph dataset. Additionally, the 140-dimensional weighted features of each brain region are used as
 270 node features. The combination of node connectivity and node features forms the foundation of the graph
 271 dataset. Finally, The training and test graph datasets were constructed according to the binary adjacency
 272 matrix and node features. It is important to note that the training set includes a validation set, which is
 273 used for both the exploration of GNN models and the prediction of SSD in the optimal GNN model. The
 274 test set is exclusively used to evaluate the performance of the optimal GNN model.

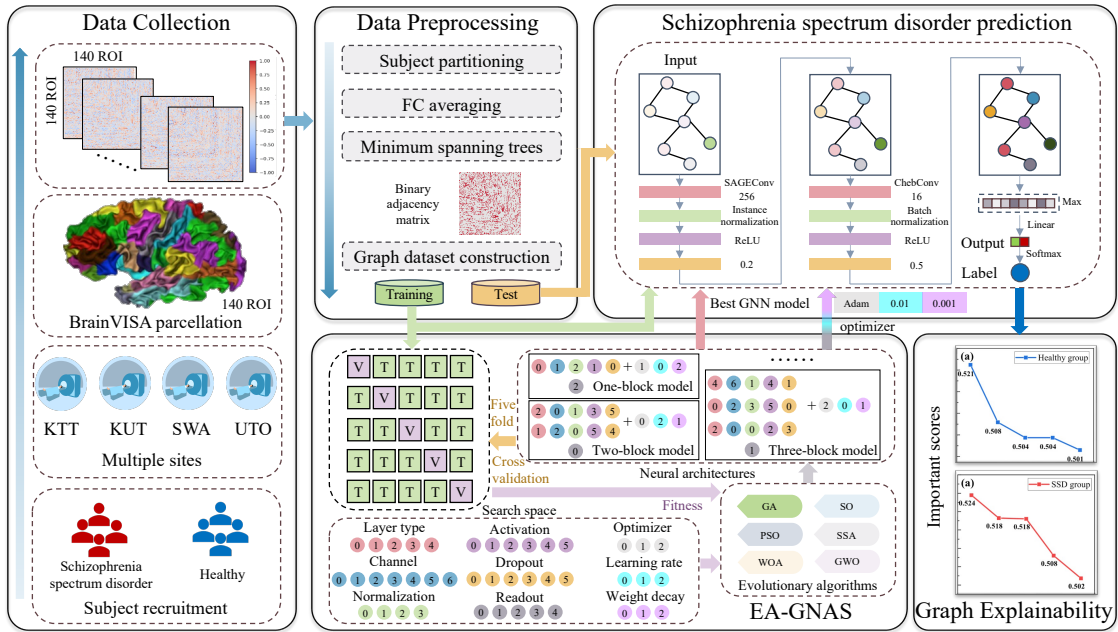


Figure 3: A generic EA-GNAS framework for SSD prediction and graph explainability.

275 4.4. Implementation details

276 Fig. 3 illustrates in detail the implementation framework of the proposed method, including data col-
 277 lection, data preprocessing, EA-GNAS, SSD prediction, and the explainability of prediction results. In the
 278 data preprocessing stage, we randomly selected 142 healthy subjects to balance the sample data, avoiding
 279 selection bias when training the GNN model. In EA-GNAS, we employed five-fold cross-validation to assess

280 model performance, set the training epochs to 10, batch size to 64, and used cross-entropy as the loss func-
 281 tion. Furthermore, we selected six popular evolutionary algorithms, namely, genetic algorithm (GA) [37],
 282 particle swarm optimization (PSO) [38], whale optimization algorithm (WOA) [46], grey wolf optimization
 283 (GWO) [47], snake optimization (SO) [42], and salp swarm algorithm (SSA) [48]. In GA, the crossover
 284 rate and mutation rate were set to 0.8 and 0.01, respectively. In PSO, the cognitive factor, social factor,
 285 and inertia weight were set to 2, 2, and 0.9, respectively. In WOA, the constant coefficient was set to 1.
 286 In SO, the two threshold values were 0.25 and 0.6, and the three constant coefficients were 0.5, 0.05, and
 287 0.5. Additionally, the learning iteration number N and the number of individuals I for all evolutionary
 288 algorithms were set to 100 and 10, respectively.

289 4.5. Comparison methods and performance metrics

290 In the comparative study of SSD prediction, we have selected four common ML methods and four DL
 291 methods mentioned in Introduction. The ML methods include SVM, KNN, RF, and LR. Among them,
 292 SVM aims to find the optimal hyperplane for classifying data points of different categories; KNN relies on
 293 distance metrics for data point classification and we set the number of nearest neighbors to 3; RF improves
 294 classification performance by combining the prediction results of multiple decision trees and we set the
 295 number of trees to 100; LR is a widely used linear model for binary classification problems, estimating the
 296 probability that an observation belongs to a certain category using a logistic function. The DL methods
 297 include BrainNetCNN [17], LGGNN [26], FCBasedGCN [25], and three other classical GNN models, namely
 298 GCN, GAT, and SAGE. Following the structure in [21], the number of layers for GCN [33], GAT [35], and
 299 SAGE [34] is set to three, with the number of features in the intermediate layers set to 128.

300 Five metrics are reported to evaluate the performance of all ML-based and DL-based SSD prediction
 301 methods. Accuracy is a measure of the overall performance of a classification model, representing the ratio
 302 of correctly predicted samples to the total number of samples, typically used when dealing with evenly
 303 distributed classes. Precision refers to the proportion of true positive samples among those predicted as
 304 positive by the model, assessing the prediction accuracy of the model. Recall is the ratio of correctly
 305 identified positive samples to the total number of true positive samples, evaluating the model's sensitivity.
 306 F1 score is the harmonic mean of precision and recall, providing a comprehensive assessment of the model's
 307 accuracy and sensitivity. The calculation formulas for these performance metrics are as follows:

$$Accuracy = \frac{TP + TN}{TP + TN + FP + FN}, \quad (6)$$

$$Precision = \frac{TP}{TP + FP}, \quad (7)$$

$$Recall = \frac{TP}{TP + FN}, \quad (8)$$

$$F1-score = 2 * \frac{Precision * Recall}{Precision + Recall}. \quad (9)$$

308 Here, TP refers to the healthy samples that are correctly classified. TN represents the SSD samples that
 309 are correctly classified. FP indicates the SSD samples that are incorrectly classified, while FN signifies the
 310 healthy samples that are incorrectly classified. In addition, the relationship between TP rate and FP rate
 311 at different thresholds can be represented by the ROC curve, and AUC represents the area under the ROC
 312 curve, typically ranging from 0 to 1, with a higher value indicating better model performance.

313 5. Results and discussions

314 In this section, we first compare the GNAS results of different evolutionary algorithms and obtain the
 315 optimal model. Secondly, we compare the SSD prediction performance of different models. Then, we conduct
 316 an explainability analysis of the GNN model. At last, the limitation of this work is discussed.

317 5.1. Parameter selection and network architecture search results

318 Fig. 4 displays the binary adjacency matrix graphs under various MST thresholds and the optimization
 319 process of various evolutionary algorithms. In this adjacency matrix, red areas represent the connections
 320 between brain regions, while non-red areas indicate no connection. The MST threshold determines the
 321 number of brain region connections, with a larger threshold resulting in more brain region connections. When
 322 the threshold is 1, it indicates that all 140 brain regions are fully connected pairwise. However, excessive
 323 connections can lead to information redundancy and increase the computational burden. Therefore, we
 324 selected three thresholds of 0.1, 0.2, and 0.3. To compare the search efficiency of each evolutionary algorithm,
 325 Fig. 4 also presents the change curves of the mean fitness of all individuals with each iteration. For a more
 326 intuitive comparison, these were processed with a moving average, with a sliding iteration number
 327 of 10. In each iteration, 10 individuals (i.e., 10 GNN models) are trained and their fitness are calculated.
 328 The mean fitness reflects the search effect of the evolutionary algorithm: the lower the value, the better
 329 the search effect. The results show that, in most cases, the mean fitness curve of SSA starts to fluctuate

330 dramatically and then gradually stabilizes, while the curve of GA converges faster, indicating that GA can
 331 find efficient GNN models and optimizers more quickly. Furthermore, all curves show a downward trend
 332 because evolutionary algorithms search based on diversity and selection. In the early stages of exploration,
 333 due to higher diversity, the algorithm will broadly explore various combinations, which may result in lower
 334 accuracy. However, as iterations progress, the algorithm will focus on high-performance areas, thereby
 335 improving accuracy.

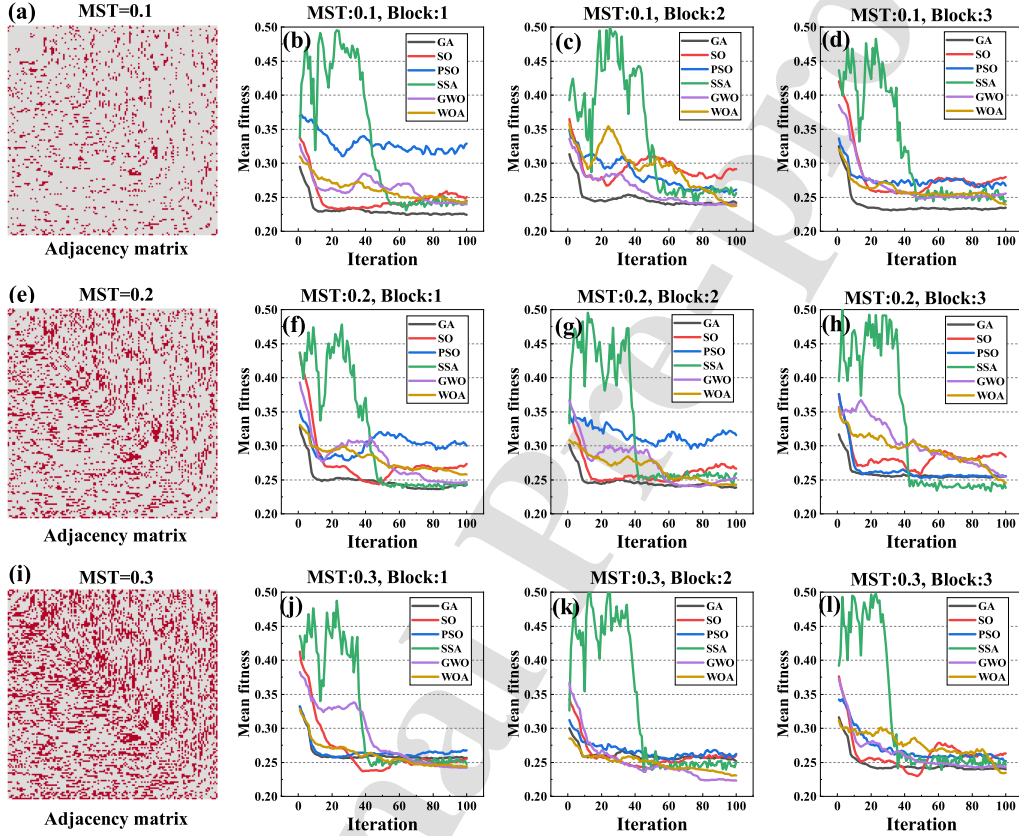


Figure 4: The curves of the mean fitness of all individuals versus iteration under different evolutionary algorithms. (a), (e), and (i) represent the adjacency matrix graphs when the MST threshold is 0.1, 0.2, and 0.3, respectively; (b) to (d) are the mean fitness values under MST 0.1 with block numbers ranging from 1 to 3; (f) to (h) are the mean fitness values under MST 0.2 with block numbers ranging from 1 to 3; (j) to (l) are the mean fitness values under MST 0.3 with block numbers ranging from 1 to 3.

336 Table 3 reports the comparison results of the best fitness obtained by six evolutionary algorithms un-
 337 der different parameter settings. The number of graph blocks typically influences the network's feature
 338 extraction performance. As shown in Table 3, an increase in the number of graph blocks leads to a certain
 339 decreasing trend in the mean fitness of the algorithms, indicating that during the GNAS process, most GNN
 340 models perform better with a larger number of graph blocks. Among all these algorithms, GA consistently

Table 3: Best fitness comparison of different evolutionary algorithms under various MST thresholds and block numbers.

EA	One-block model			Two-block model			Three-block model		
	MST=0.1	MST=0.2	MST=0.3	MST=0.1	MST=0.2	MST=0.3	MST=0.1	MST=0.2	MST=0.3
SSA	0.2028	0.2202	0.2161	0.2071	0.2204	0.2028	0.2071	0.2114	0.1895
WOA	0.2024	0.2072	0.2069	0.2025	0.2116	0.1895	0.2072	0.2027	0.1853
GWO	0.2163	0.2207	0.2290	0.2026	0.2070	0.1938	0.2023	0.2026	0.2073
PSO	0.1983	0.2073	0.2073	0.2026	0.1899	0.2116	0.1894	0.2070	0.1984
SO	0.2027	0.2159	0.2069	0.1853	0.2026	0.2071	0.1897	0.1942	0.1984
GA	0.1895	0.2027	0.1985	0.1939	0.1850	0.1939	0.1851	0.1939	0.2026
Mean	0.2020	0.2123	0.2108	0.1990	0.2028	0.1998	0.1968	0.2020	0.1969

341 demonstrates superior performance across multiple settings, achieving the best fitness values in both the
342 one-block and three-block models at most MST thresholds. This implies that GA has the the better robust-
343 ness and adaptability to varied model complexities and threshold constraints in GNAS. Conversely, while
344 algorithms like WOA and SO exhibit optimal performance in specific scenarios (e.g., SO for the two-block
345 model at MST=0.1 and WOA for the three-block model at MST=0.3), their efficacy isn't consistent across
346 the board. As a result, we select the GNN model and optimizer found by GA with MST=0.2 and block=2
347 for subsequent SSD prediction comparisons, at which point the best fitness reaches its lowest at 0.1850.

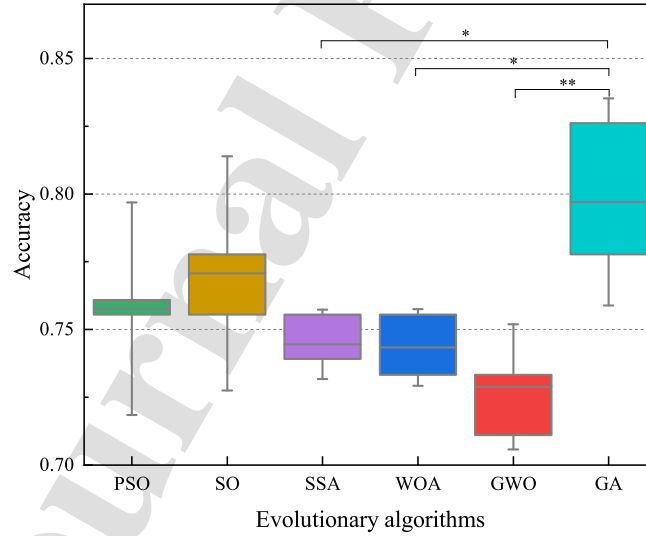


Figure 5: Validation accuracy boxplots of the GNN models searched by six evolutionary algorithms. The t-test was applied to compare GA with other algorithms. The one asterisk * and two asterisks ** denote $0.01 < p \leq 0.05$ and $p \leq 0.01$, respectively

348 Fig. 5 compares the validation accuracies of the optimal models obtained during the search process by

349 different evolutionary algorithms. The t-test is employed to compare whether there is a significant difference
 350 between the accuracies of the two sample groups. The findings reveals that the average accuracy of the
 351 GNN model obtained through the GA search process is close to 0.80, substantially surpassing the average
 352 accuracies of the GNN models derived from other algorithmic searches. Meanwhile, the results yielded by
 353 the GA exhibits statistically significant deviations from those of the SSA, WOA, and GWO algorithms
 354 ($p \leq 0.05$).

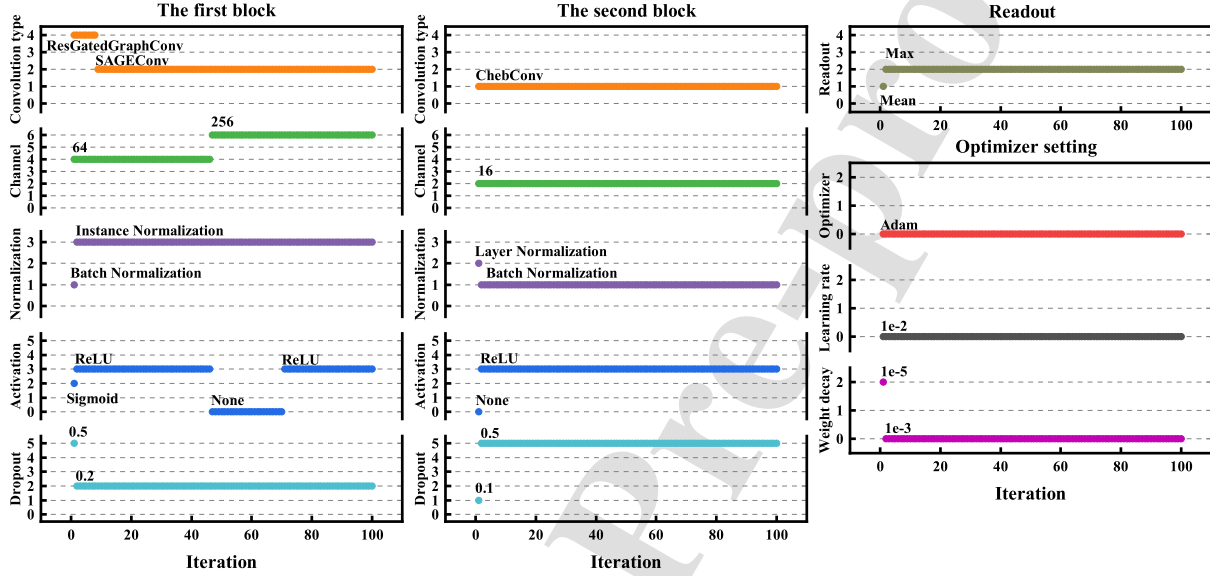


Figure 6: The search process of all components in the optimal architecture obtained through GA-GNAS.

355 Fig. 6 shows the changes in the components of the best architecture during the GNAS process with
 356 GA. Most components, such as the optimizer and layers in the second block, are determined in the early
 357 stages of exploration, indicating that these specific components provide a significant performance boost to
 358 the network. At the same time, some components in the first block only stabilize after the middle of the
 359 exploration phase. This suggest that the algorithm might get stuck in a local optimum initially but later
 360 jumps out in search of a better solution. Therefore, in the early stages of the search, the evolutionary
 361 algorithm determines the main structure of the network, and afterwards, it continuously optimizes the
 362 construction details of the architecture.

363 To further demonstrate the differences among the GNN models searched by different evolutionary al-
 364 gorithms, Table 4 reports their performance on the SSD prediction task. Bold values indicate the best
 365 scores, while underlined values denote the second-best scores. The GNN model searched by GA achieves

366 an accuracy of 0.8246, a recall of 0.8182, an F1 score of 0.8438, and an AUC of 0.8258, performing the
 367 best overall. The model searched by WOA has the highest precision of 0.8800. According to the accuracy
 368 and comprehensive metric AUC, on this SSD prediction task, the GNN model searched by GA outperforms
 369 those by other algorithms, followed by SO, while GWO performs the worst. The results are consistent with
 370 the cross-validation results in Fig. 5.

Table 4: Comparison results of performance metrics for the GNN models searched by different evolutionary algorithms

EA	Accuracy	Precision	Recall	F1 score	AUC
SSA	0.7544	0.8519	0.6970	<u>0.7667</u>	0.7652
WOA	0.7544	0.8800	0.6667	0.7586	0.7708
GWO	0.7193	0.8400	0.7241	0.6364	0.7348
PSO	0.7719	0.8333	0.7937	0.7576	0.7746
SO	<u>0.7895</u>	0.8621	<u>0.7955</u>	0.7576	<u>0.8065</u>
GA	0.8246	<u>0.8710</u>	0.8182	0.8438	0.8258

371 5.2. Comparison results with baseline methods

Table 5: Comparison results of performance metrics for different methods.

Methods	Accuracy	Precision	Recall	F1 score	AUC	
ML-based	SVM [6]	0.7368	0.8462	0.6667	0.7458	0.7500
	KNN [14]	0.6491	0.8421	0.4848	0.6154	0.6799
	RF [11]	0.6667	0.8500	0.5152	0.6415	0.6951
	LR [11]	0.7368	<u>0.8750</u>	0.6364	0.7368	0.7557
DL-based	BrainNetCNN [17]	0.7719	0.7632	0.8788	<u>0.8169</u>	0.7519
	GCN [33]	0.7368	0.7647	0.7879	0.7761	0.7273
	GAT [35]	0.7544	0.7879	0.7879	0.7879	0.7481
	SAGE [34]	0.7544	0.8276	0.7273	0.7742	0.7595
	FCBasedGCN [25]	0.7368	0.7368	<u>0.8485</u>	0.7887	0.7159
	LGGNN [26]	<u>0.8070</u>	0.8846	0.7419	0.8070	<u>0.8133</u>
	GA-GNAS (Ours)	0.8246	0.8710	0.8182	0.8438	0.8258

372 Table 5 reports the performance metrics of various ML-based and DL-based methods. Among the ML-
 373 based methods, LR has the highest precision of 0.8750, while SVM and LR both achieve the same top
 374 accuracy of 0.7368. KNN performs the worst among all ML-based methods. Among the DL-based methods,
 375 GA-GNAS outperforms others in terms of accuracy, F1 score, and AUC. LGGNN has the highest precision
 376 of 0.8846, and ranks second in accuracy and AUC. However, this method’s recall is not outstanding, implying

377 that its predictions may result in more false negatives. Overall, GA-GNAS displays balanced performance
378 across all metrics, indicating that it can provide robust prediction results under various evaluation conditions.
379 Such balance is particularly important for practical applications because it ensures reliable predictions in
380 various scenarios and conditions.

381 In this study, the GNN-based methods outperforms traditional machine learning methods in most eval-
382 uation metrics. This phenomenon is primarily because the connections between brain regions exhibit clear
383 spatial structures and interdependent characteristics. GNN can capture long-distance dependencies through
384 iterative node updates and message-passing mechanisms, thus fully utilizing the relational information in
385 these structured data, enhancing the results of SSD prediction. Additionally, the proposed method shows
386 superior performance compared to hand-crafted GNN models. This superiority is mainly because hand-
387 crafted architectures are often limited by the designer’s experience and prior knowledge, whereas evolution-
388 ary algorithms are not constrained by these factors. They can explore excellent architectures that human
389 designers might overlook or not consider. Therefore, using evolutionary algorithms can not only obtain a
390 high-performance GNN model for SSD prediction but also save the time and effort required for manually
391 designing and adjusting GNN models.

392 *5.3. Explainability analysis of the GNN models*

393 Although the proposed methods and some comparative methods can effectively distinguish between
394 the healthy group and the SSD group, the key factors behind the inference of these models remain un-
395 clear. Therefore, we utilized the GNNExplainer method for explainability analysis of GNN models. Since
396 GNNExplainer is a technique specifically designed for the explainability analysis of the GNN model, and
397 BrainNetCNN and ML-based methods are not GNN models, we did not perform explainability analysis on
398 them. BrainVISA has defined 140 brain regions, and we present the top five brain regions that have the
399 greatest impact on the different GNN models for both the healthy group and the SSD group, as shown in
400 Figs. 7 and 8. The x-axis represents the brain region annotations defined by BrainVISA, and the y-axis
401 represents the importance scores of each brain region. It is found that the brain regions of interest differ
402 among models, yet there are similarities. For the healthy group, GCN, SAGE, and LGGNN all identify
403 the Intraparietal Sulcus (brain regions abbreviated with F.I.P) and Pallidum as two important areas. GAT
404 and FCBasedGCN both recognize the Thalamus as having a high impact. For the SSD group, the Ven-
405 tricle is very important for predicting SSD, identified by all GNN models. This is consistent with existing
406 research indicating that ventricle enlargement is a key indicator for diagnosing SSD [49, 50]. Additionally,
407 the Temporal Sulcus (brain regions abbreviated with S.T.) reveals another piece of evidence impacting the

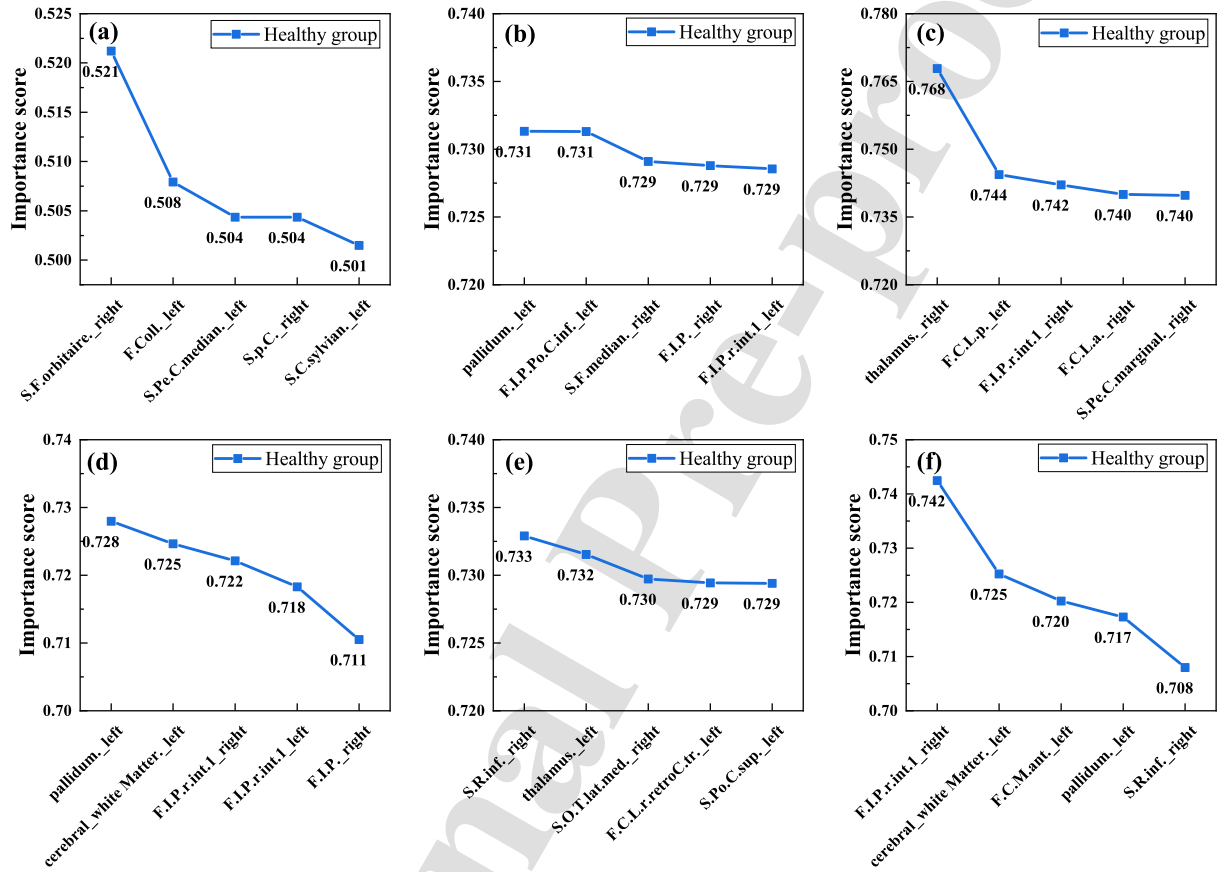


Figure 7: Results of the GNNExplainer methods under different GNN models in the healthy group. From (a) to (f) are the results of GA-GNAS, GCN, GAT, SAGE, FCBasedGCN, and LGGNN, respectively.

408 identification of SSD. This finding is consistent with research reporting differences in the connectivity of
 409 the posterior superior temporal sulcus in social cognition between SSD patients and healthy individuals
 410 [51]. Other brain regions identified by the GNN models may also be meaningful for the diagnosis of SSD,
 411 providing valuable references for neuroscientists.

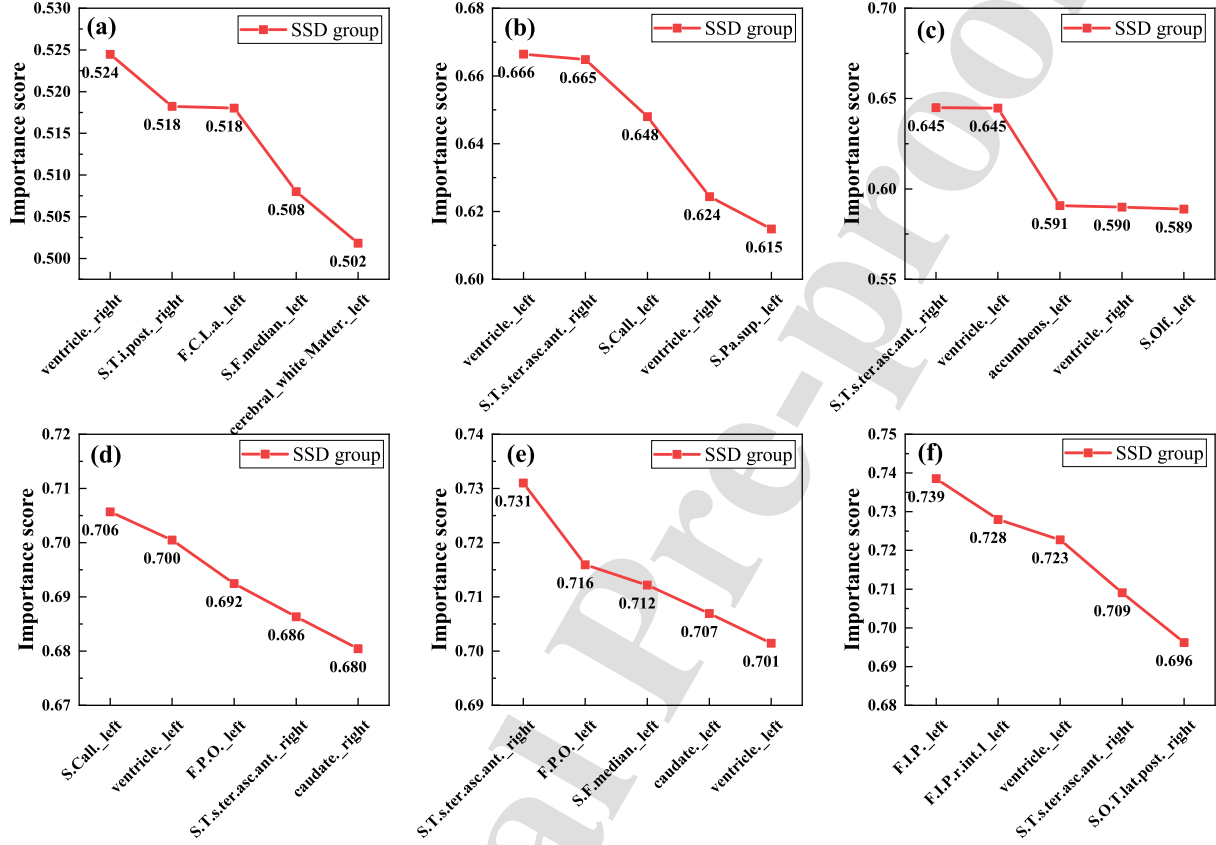


Figure 8: Results of the GNNExplainer methods under different GNN models in the SSD group. From (a) to (f) are the results of GA-GNAS, GCN, GAT, SAGE, FCBasedGCN, and LGGNN, respectively.

412 5.4. Limitation

413 Although this study proposes an effective deep learning method for accurately predicting SSD, there are
 414 still some limitations. On one hand, the size of the dataset we used may not be sufficient to capture all
 415 the complexities of SSD. A smaller dataset might lead to model overfitting, reducing its generalizability on
 416 broader and more diverse data. On the other hand, we conducted experimental comparisons of MST and
 417 graph block at different values and selected the GNN model searched by GA-GNAS with MST at 0.2 and
 418 graph block at 2. This parameter combination is predefined and might not be optimal, potentially limiting

419 enhancements to the model's performance. Therefore, future research will consider using larger datasets to
420 increase data diversity and further optimizing and expanding the search space to overcome these limitation.

421 **6. Conclusion**

422 In this study, we propose a novel framework, EA-GNAS, to search for an optimal GNN model and its
423 associated optimizer. This model aims to classify SSD patients and healthy individuals using rs-fMRI data.
424 Specifically, we compare multiple evolutionary algorithms, with GA demonstrating superior performance
425 in the majority of cases. Additionally, when juxtaposed with conventional ML techniques and other DL
426 methodologies, GA-GNAS exhibits enhanced performance in accuracy, F1-score, and AUC metrics. These
427 comparative findings underscore the efficacy and robustness of the proposed method. Furthermore, we
428 employ GNNExplainer to illustrate which brain regions and connections the GNN model pays more attention
429 to when classifying SSD patients and healthy individuals. This offers valuable insights for neuroscientists
430 delving into SSD analysis.

431 **Conflict of interest**

432 The authors declared that they have no conflicts of interest to this work.

433 **Acknowledgement**

434 The authors would like to thank China Scholarship Council for supporting this work. S. H. work was
435 carried out as part of the doctoral programme in Experimental Sciences and Technology at the University
436 of Vic - Central University of Catalonia.

437 **Funding**

438 This work was supported by the National Key R&D Program of China (No. 2017YFE0129700) and
439 China Scholarship Council (No. 202206690046).

440 **Authors' Contributions:**

441 All authors contributed to the study conception and design. Experiment preparation, data collection
442 and analysis were performed by Shurun Wang, Shuning Han. The first draft of the manuscript was written
443 by Shurun Wang and all authors commented on previous versions of the manuscript. All authors read and
444 approved the final manuscript.

445 **References**

- 446 [1] H. Y. Chong, S. L. Teoh, D. B.-C. Wu, S. Kotirum, C.-F. Chiou, N. Chaiyakunapruk, Global economic burden of
 447 schizophrenia: a systematic review, *Neuropsych. Dis. Treat.* (2016) 357–373.
- 448 [2] K. R. Patel, J. Cherian, K. Gohil, D. Atkinson, Schizophrenia: overview and treatment options, *Pharm. Ther.* 39 (9)
 449 (2014) 638.
- 450 [3] M. Dabiri, F. Dehghani Firouzabadi, K. Yang, P. B. Barker, R. R. Lee, D. M. Yousem, Neuroimaging in schizophrenia:
 451 A review article, *Front. Neurosci.* 16 (2022) 1042814.
- 452 [4] L. Attademo, F. Bernardini, N. Verdolini, Neural correlates of schizotypal personality disorder: a systematic review of
 453 neuroimaging and eeg studies, *Curr. Med. Imaging* 17 (11) (2021) 1283–1298.
- 454 [5] C. Cruz-Martinez, C. A. Reyes-Garcia, N. Vanello, A novel event-related fMRI supervoxels-based representation and its
 455 application to schizophrenia diagnosis, *Comput. Meth. Prog. Bio.* 213 (2022) 106509.
- 456 [6] X. Ma, W. F. Z. Yang, W. Zheng, Z. Li, J. Tang, L. Yuan, L. Ouyang, Y. Wang, C. Li, K. Jin, et al., Neuronal dysfunction
 457 in individuals at early stage of schizophrenia, a resting-state fmri study, *Psychiat. Res.* 322 (2023) 115123.
- 458 [7] I. Gallos, L. Mantonakis, E. Spilioti, E. Kattoulas, E. Savvidou, E. Anyfandi, E. Karavasilis, N. Kelekis, N. Smyrnis,
 459 C. Siettos, The relation of integrated psychological therapy to resting state functional brain connectivity networks in
 460 patients with schizophrenia, *Psychiat. Res.* 306 (2021) 114270.
- 461 [8] Y. Du, X. He, P. Kochunov, G. Pearlson, L. E. Hong, T. G. van Erp, A. Belger, V. D. Calhoun, A new multimodality
 462 fusion classification approach to explore the uniqueness of schizophrenia and autism spectrum disorder, *Hum. Brain Mapp.*
 463 43 (12) (2022) 3887–3903.
- 464 [9] S. Ramkiran, A. Sharma, N. P. Rao, Resting-state anticorrelated networks in schizophrenia, *Psychiat. Res. Neuroim.* 284
 465 (2019) 1–8.
- 466 [10] Y. Gao, X. Tong, J. Hu, H. Huang, T. Guo, G. Wang, Y. Li, G. Wang, Decreased resting-state neural signal in the left
 467 angular gyrus as a potential neuroimaging biomarker of schizophrenia: an amplitude of low-frequency fluctuation and
 468 support vector machine analysis, *Front. Psychiatry* 13 (2022) 949512.
- 469 [11] S. Srinivasagopalan, J. Barry, V. Gurupur, S. Thankachan, A deep learning approach for diagnosing schizophrenic patients,
 470 *J. Exp. Theor. Artif. In.* 31 (6) (2019) 803–816.
- 471 [12] W. Zhu, S. Shen, Z. Zhang, Improved multiclassification of schizophrenia based on xgboost and information fusion for
 472 small datasets, *Comput. Math. Method. M.* 2022 (2022).
- 473 [13] M. Sharma, R. K. Patel, A. Garg, R.-S. Tan, U. R. Acharya, Automated detection of schizophrenia using deep learning:
 474 a review for the last decade, *Physiol. Meas.* (2023).
- 475 [14] J. R. de Miras, A. J. Ibáñez-Molina, M. F. Soriano, S. Iglesias-Parro, Schizophrenia classification using machine learning
 476 on resting state EEG signal, *Biomed. Signal Proces.* 79 (2023) 104233.
- 477 [15] D. Sadeghi, A. Shoeibi, N. Ghassemi, P. Moridian, A. Khadem, R. Alizadehsani, M. Teshnehlab, J. M. Gorriz,
 478 F. Khozeimeh, Y.-D. Zhang, et al., An overview of artificial intelligence techniques for diagnosis of schizophrenia based on
 479 magnetic resonance imaging modalities: Methods, challenges, and future works, *Comput. Biol. Med.* 146 (2022) 105554.
- 480 [16] L.-L. Zeng, Z. Fan, J. Su, M. Gan, L. Peng, H. Shen, D. Hu, Gradient matching federated domain adaptation for brain
 481 image classification, *IEEE T. Neur. Net. Lear.* (2022).
- 482 [17] J. Kawahara, C. J. Brown, S. P. Miller, B. G. Booth, V. Chau, R. E. Grunau, J. G. Zwicker, G. Hamarneh, BrainNetCNN:

- 483 Convolutional neural networks for brain networks; towards predicting neurodevelopment, *NeuroImage* 146 (2017) 1038–
 484 1049.
- 485 [18] A. Gupta, R. Daniel, A. Rao, P. P. Roy, S. Chandra, B.-G. Kim, Raw electroencephalogram-based cognitive workload
 486 classification using directed and nondirected functional connectivity analysis and deep learning, *Big Data* (2023).
- 487 [19] X. Chen, B. Li, H. Jia, F. Feng, F. Duan, Z. Sun, C. F. Caiafa, J. Solé-Casals, Graph empirical mode decomposition-based
 488 data augmentation applied to gifted children mri analysis, *Front. Neurosci.* 16 (2022) 866735.
- 489 [20] K.-H. Oh, I.-S. Oh, U. Tsogt, J. Shen, W.-S. Kim, C. Liu, N.-I. Kang, K.-H. Lee, J. Sui, S.-W. Kim, et al., Diagnosis
 490 of schizophrenia with functional connectome data: a graph-based convolutional neural network approach, *BMC Neurosci.*
 491 23 (1) (2022) 1–11.
- 492 [21] X. Chen, J. Zhou, P. Ke, J. Huang, D. Xiong, Y. Huang, G. Ma, Y. Ning, F. Wu, K. Wu, Classification of schizophrenia
 493 patients using a graph convolutional network: a combined functional MRI and connectomics analysis, *Biomed. Signal*
 494 *Proces.* 80 (2023) 104293.
- 495 [22] R. Yu, C. Pan, X. Fei, M. Chen, D. Shen, Multi-graph attention networks with bilinear convolution for diagnosis of
 496 schizophrenia, *IEEE J. Biomed. Health.* 27 (3) (2023) 1443–1454.
- 497 [23] M. Liu, H. Zhang, F. Shi, D. Shen, Hierarchical graph convolutional network built by multiscale atlases for brain disorder
 498 diagnosis using functional connectivity, *IEEE T. Neur. Net. Lear.* (2023).
- 499 [24] E. N. Pitsik, V. A. Maximenko, S. A. Kurkin, A. P. Sergeev, D. Stoyanov, R. Paunova, S. Kandilarova, D. Simeonova, A. E.
 500 Hramov, The topology of fMRI-based networks defines the performance of a graph neural network for the classification of
 501 patients with major depressive disorder, *Chaos, Soliton. Fract.* 167 (2023) 113041.
- 502 [25] S. Han, Z. Sun, K. Zhao, F. Duan, C. F. Caiafa, Y. Zhang, J. Solé-Casals, Early prediction of dementia using fMRI data
 503 with a graph convolutional network approach, *J. Neural Eng.* 21 (1) (2024) 016013.
- 504 [26] H. Zhang, R. Song, L. Wang, L. Zhang, D. Wang, C. Wang, W. Zhang, Classification of brain disorders in rs-fMRI via
 505 local-to-global graph neural networks, *IEEE T. Med. Imaging* 42 (2) (2022) 444–455.
- 506 [27] Z. Lu, I. Whalen, Y. Dhebar, K. Deb, E. D. Goodman, W. Banzhaf, V. N. Boddeti, Multiobjective evolutionary design of
 507 deep convolutional neural networks for image classification, *IEEE T. Evolut. Comput.* 25 (2) (2020) 277–291.
- 508 [28] D. Sapra, A. D. Pimentel, Designing convolutional neural networks with constrained evolutionary piecemeal training,
 509 *Appl. Intell.* 52 (15) (2022) 17103–17117.
- 510 [29] Y. Gao, H. Yang, P. Zhang, C. Zhou, Y. Hu, Graphnas: Graph neural architecture search with reinforcement learning,
 511 arXiv preprint arXiv:1904.09981 (2019).
- 512 [30] K. Zhou, X. Huang, Q. Song, R. Chen, X. Hu, Auto-gnn: Neural architecture search of graph neural networks, *Front. in*
 513 *big Data* 5 (2022) 1029307.
- 514 [31] J. Chen, J. Gao, Y. Chen, B. M. Oloulade, T. Lyu, Z. Li, Auto-GNAS: A parallel graph neural architecture search
 515 framework, *IEEE T. Parall. Distr.* 33 (11) (2022) 3117–3128.
- 516 [32] M. Shi, Y. Tang, X. Zhu, Y. Huang, D. Wilson, Y. Zhuang, J. Liu, Genetic-gnn: Evolutionary architecture search for
 517 graph neural networks, *Knowl. Based Syst.* 247 (2022) 108752.
- 518 [33] T. N. Kipf, M. Welling, Semi-supervised classification with graph convolutional networks, in: *Proceedings of the 5th*
 519 *International Conference on Learning Representations*, 2017.
- 520 [34] W. Hamilton, Z. Ying, J. Leskovec, Inductive representation learning on large graphs, in: *Advances in neural information*
 521 *processing systems*, Vol. 30, 2017.

- 522 [35] P. Veličković, G. Cucurull, A. Casanova, A. Romero, P. Liò, Y. Bengio, Graph attention networks, in: International
523 Conference on Learning Representations, 2018.
- 524 [36] R. Li, X. Yuan, M. Radfar, P. Marendy, W. Ni, T. J. O'Brien, P. M. Casillas-Espinosa, Graph signal processing, graph
525 neural network and graph learning on biological data: a systematic review, *IEEE Rev. Biomed. Eng.* (2021).
- 526 [37] J. H. Holland, Genetic algorithms, *Sci. Am.* 267 (1) (1992) 66–73.
- 527 [38] J. Kennedy, R. Eberhart, Particle swarm optimization, in: Proceedings of ICNN'95-international conference on neural
528 networks, Vol. 4, IEEE, 1995, pp. 1942–1948.
- 529 [39] Z. Ying, D. Bourgeois, J. You, M. Zitnik, J. Leskovec, GNNExplainer: Generating explanations for graph neural networks,
530 in: Advances in Neural Information Processing Systems, Vol. 32, 2019.
- 531 [40] M. Defferrard, X. Bresson, P. Vandergheynst, Convolutional neural networks on graphs with fast localized spectral filtering,
532 in: Advances in Neural Information Processing Systems, Vol. 29, 2016.
- 533 [41] X. Bresson, T. Laurent, Residual gated graph convnets, ArXiv Preprint ArXiv:1711.07553 (2017).
- 534 [42] F. A. Hashim, A. G. Hussien, Snake optimizer: A novel meta-heuristic optimization algorithm, *Knowl. Based Syst.* 242
535 (2022) 108320.
- 536 [43] S. C. Tanaka, A. Yamashita, N. Yahata, T. Itahashi, G. Lisi, T. Yamada, N. Ichikawa, M. Takamura, Y. Yoshihara,
537 A. Kunimatsu, et al., A multi-site, multi-disorder resting-state magnetic resonance image database, *Sci. Data* 8 (1) (2021)
538 227.
- 539 [44] M. Perrot, D. Rivière, J.-F. Mangin, Cortical sulci recognition and spatial normalization, *Med. Image Anal.* 15 (4) (2011)
540 529–550.
- 541 [45] C. Stam, P. Tewarie, E. Van Dellen, E. Van Straaten, A. Hillebrand, P. Van Mieghem, The trees and the forest: charac-
542 terization of complex brain networks with minimum spanning trees, *Int. J. Psychophysiol.* 92 (3) (2014) 129–138.
- 543 [46] S. Mirjalili, A. Lewis, The whale optimization algorithm, *Adv. Eng. Softw.* 95 (2016) 51–67.
- 544 [47] S. Mirjalili, S. M. Mirjalili, A. Lewis, Grey wolf optimizer, *Adv. Eng. Softw.* 69 (2014) 46–61.
- 545 [48] S. Mirjalili, A. H. Gandomi, S. Z. Mirjalili, S. Saremi, H. Faris, S. M. Mirjalili, Salp swarm algorithm: A bio-inspired
546 optimizer for engineering design problems, *Adv. Eng. Softw.* 114 (2017) 163–191.
- 547 [49] T.-Y. Eom, S. B. Han, J. Kim, J. A. Blundon, Y.-D. Wang, J. Yu, K. Anderson, D. B. Kaminski, S. M. Sakurada, S. M.
548 Pruett-Miller, et al., Schizophrenia-related microdeletion causes defective ciliary motility and brain ventricle enlargement
549 via microRNA-dependent mechanisms in mice, *Nat. Commun.* 11 (1) (2020) 912.
- 550 [50] B. Franke, J. L. Stein, S. Ripke, V. Anttila, D. P. Hibar, K. J. Van Huzen, A. Arias-Vasquez, J. W. Smoller, T. E. Nichols,
551 M. C. Neale, et al., Genetic influences on schizophrenia and subcortical brain volumes: large-scale proof of concept, *Nat.*
552 *Neurosci.* 19 (3) (2016) 420–431.
- 553 [51] D. Mier, S. Eisenacher, F. Rausch, S. Englisch, M. F. Gerchen, V. Zamoscik, A. Meyer-Lindenberg, M. Zink, P. Kirsch,
554 Aberrant activity and connectivity of the posterior superior temporal sulcus during social cognition in schizophrenia, *Eur.*
555 *Arch. Psy. Clin. N.* 267 (7) (2017) 597–610.

Highlights

- We propose a generic graph neural architecture search framework based on the evolutionary algorithm to construct GNN model for schizophrenia spectrum disorder prediction.
- We compare our model with other popular machine learning and deep learning models on multi-site datasets.
- We introduce the GNNE explainer method to provide the explainability results for the model prediction.
- The explainability analysis results provide valuable insights for future diagnosis and treatment
- The source code is publicly available on GitHub at <https://github.com/Shurun-Wang/EA-GNAS>.

The authors declare that they have no known competing financial interests or personal relationships that could have appeared to influence the work reported in this paper.

Journal Pre-proof